PROCEEDINGS OF SCIENCE

Nucleon form factors and structure functions with N_f=2+1 dynamical domain wall fermions

Takeshi Yamazaki[*]
University of Connecticut, Physics Department, Storrs, Connecticut 06269-3046, USA
yamazaki@phys.uconn.edu

Shigemi Ohta[†]
Institute of Particle and Nuclear Studies, KEK, Tsukuba, Ibaraki 305-0801, Japan
RIKEN-BNL Research Center, Brookhaven National Laboratory, Upton, NY 11973
Physics Department, Sokendai Graduate U. Adv. Studies, Hayama, Kanagawa 240-0193, Japan
shigemi.ohta@kek.jp

RBC and UKQCD Collaborations

We report isovector form factors and low moments of structure functions of nucleon in numerical lattice quantum chromodynamics (QCD) from the on-going calculations by the RIKEN-BNL-Columbia (RBC) and UKQCD Collaborations with (2+1) dynamical flavors of domain-wall fermion (DWF) quarks. We calculate the matrix elements with four light quark masses, corresponding to pion mass values of $m_\pi = 330$–670 MeV, while the dynamical strange mass is fixed at a value close to physical, on $(2.7\ \mathrm{fm})^3$ spatial volume. We found that our axial charge, g_A, at the lightest mass exhibits a large deviation from the heavier mass results. This deviation seems to be a finite-size effect as the g_A value scales with a single parameter, $m_\pi L$, the product of pion mass and linear spatial lattice size. The scaling is also seen in earlier 2-flavor dynamical DWF and Wilson quark calculations. Without this lightest point, the three heavier mass results show only very mild mass dependence and linearly extrapolate to $g_A = 1.16(6)$. We determined the four form factors, the vector (Dirac), induced tensor (Pauli), axial vector and induced pseudoscalar, at a few finite momentum transfer values as well. At the physical pion mass the form-factors root mean square radii determined from the momentum-transfer dependence are 20–30% smaller than the corresonding experiments. The ratio of the isovector quark momentum to helicity fractions, $\langle x\rangle_{u-d}/\langle x\rangle_{\Delta u-\Delta d}$ is in agreement with experiment without much mass dependence including the lightest point. We obtain an estimate, 0.81(2), by a constant fit. Although the individual momentum and helicity fractions are yet to be renormalized, they show encouraging trend toward experiment.

The XXV International Symposium on Lattice Field Theory
July 30 - August 4 2007
Regensburg, Germany

[*]Speaker for Nucleon form factors with N_f=2+1 domain wall fermions
[†]Speaker for Nucleon structure functions with N_f =2+1 dynamical domain-wall fermions

PoS(LATTICE 2007)165

1. Introduction

We report isovector form factors and low moments of structure functions of nucleon in numerical lattice quantum chromodynamics (QCD) from the on-going calculations by the RIKEN-BNL-Columbia (RBC) and UKQCD Collaborations [1 – 3] with degenerate up and down and a heavier strange flavors represented by domain-wall fermions (DWF) [4 – 6].

The isovector form factors are defined in the following two equations:

$$\langle p|V_\mu(0)|p\rangle = \overline{u}_p\left[\gamma_\mu F_1(q^2)+\sigma_{\mu\nu}q_\nu F_2(q^2)/2m_N\right]u_p, \tag{1.1}$$

$$\langle p|A_\mu(0)|p\rangle = \overline{u}_p\left[\gamma_\mu\gamma_5 G_A(q^2)+iq_\mu\gamma_5 G_P(q^2)\right]u_p, \tag{1.2}$$

where $V_\mu=\overline{u}\gamma_\mu u-\overline{d}\gamma_\mu d$ and $A_\mu=\overline{u}\gamma_\mu\gamma_5 u-\overline{d}\gamma_\mu\gamma_5 d$ are isovector vector and axial vector currents, respectively. These form factors are experimentally measured in neutron decays and other electroweak transitions of nucleon [7]. All the form factors can be calculated numerically on the lattice [8, 9].

The structure functions are measured in deep inelastic lepton scatterings off nucleon [7]. For their definitions we refer the readers to an earlier RBC publication [10] and references cited there in. In this report we discuss some of their isovector low moments such as the momentum fraction $\langle x\rangle_{u-d}$, helicity fraction $\langle x\rangle_{\Delta u-\Delta d}$, transversity $\langle 1\rangle_{\delta u-\delta d}$ and twist-3 d_1.

2. Formulation

The matrix elements corresponding to linear combinations of the form factors eqs.(1.1) and (1.2) are determined from the ratio of the three-point and two-point functions [11]

$$R_\mu^{\mathscr{O},\mathscr{P}}(t,\mathbf{q})=\frac{G_\mu^{\mathscr{O},\mathscr{P}}(t,\mathbf{q})}{G_2^G(t'-t_0,\mathbf{0})}\left[\frac{G_2^L(t'-t,\mathbf{q})G_2^G(t-t_0,\mathbf{0})G_2^L(t'-t_0,\mathbf{0})}{G_2^L(t'-t,\mathbf{0})G_2^G(t-t_0,\mathbf{q})G_2^L(t'-t_0,\mathbf{q})}\right]^{\frac{1}{2}}, \tag{2.1}$$

where $G_\mu^{\mathscr{O},\mathscr{P}}(t,\mathbf{q})$ is three-point function,

$$G_\mu^{\mathscr{O},\mathscr{P}}(t,\mathbf{q})=\frac{1}{4}\mathrm{Tr}\left[\mathscr{P}\langle 0|\chi(t',\mathbf{0})\mathscr{O}(t,\mathbf{q})\overline{\chi}(t_0,-\mathbf{q})\rangle\right], \tag{2.2}$$

with the current $\mathscr{O}=V_\mu,A_\mu$, the projector $\mathscr{P}=\frac{1+\gamma_t}{2}(\mathscr{P}_t),\frac{1+\gamma_t}{2}\gamma_5\gamma_z(\mathscr{P}_{5z})$, the spatial momentum transfer $\mathbf{q}$, and χ being the nucleon field. t_0 and t' are the sources of the three-point function, and $G_2^{L,G}$ is the two-point function with the point(L) or the gauge invariant Gaussian smearing(G) operator sink. All the sources for the two- and three-point functions are calculated with the gauge invariant Gaussian smearing operator. $R_\mu^{\mathscr{O},\mathscr{P}}(t)$ at $t_0\ll t\ll t'$ will be constant, and corresponds to the linear combination of the form factors multiplied by kinematic factors. The form factor is obtained by solving the linear equation. The details of the equations are in Ref. [9].

The axial charge is calculated by the ratio of the three-point function $G_z^{A,\mathscr{P}_{5z}}(t)/G_t^{V,\mathscr{P}_t}(t)=Z_V g_A/Z_A$ at zero momentum transfer. This ratio gives the renomalized axial charge g_A, because the axialvector and vector currents share a common renormalization, $Z_A=Z_V$, up to second order

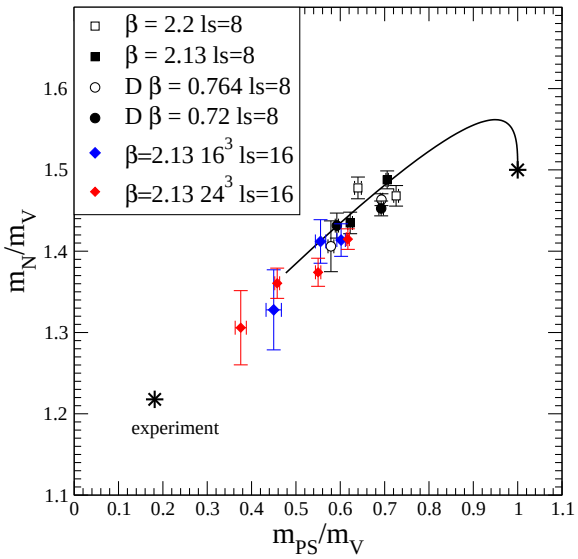

Figure 1: An Edinburgh plot obtained from the present and related RBC and UKQCD joint ensembles with (2+1)-flavor dynamical DWF quarks.

discretization error thanks to the well-preserved chiral symmetry of the domain wall fermions. We confirm that these renormalization constants agree within 0.5% accuracy in the chiral limit.

The matrix elements related to the structure functions, such as the momentum fraction, helicity distribution, moment of transversity and d_1, are calculated by the ratio of the three-point function to the two-point function, $G^{\mathscr{O}',\mathscr{P}}(t)/G_2^G(t')$, at zero momentum transfer. Definitions of the operators $\mathscr{O}'$ are listed in detail in Ref. [10]. At the lightest quark mass $m_f = 0.005$ the three-point function with the temporal direction of the conserved vector current [12] $\mathscr{V}_t$ at $\mathbf{q} = 0$ is used for the denominator of the ratio instead of $G_2^G(t')$. This ratio gives same matrix element because a relation, $G_t^{\mathscr{V},\mathscr{P}_t}(t)/G_2^G(t') = 1$, is satisfied for $t_0 \ll t \ll t'$.

3. Numerical setup

The calculations are performed on the QCDOC dedicated computers [13] at RIKEN-BNL Research Center (RBRC) and University of Edinburgh. Descriptions of the ensembles used are found in RBC-UKQCD publications [1–3]. We use a combination of Iwasaki rectangular gauge action [14] with the gauge coupling set at 2.13 and domain-wall fermion [4–6] quarks with the domain-wall height set at 1.8. A $24^3 \times 64$ lattice is used. We fix the dynamical strange mass at 0.04 and generated four different ensembles with degenerate up and down mass each at 0.03, 0.02, 0.01 and 0.005 in lattice units. From these we estimate the lattice cut off to be about a^{-1} of 1.73(3) GeV [15] with the Ω^- baryon mass. The 24^3 lattice spatial volume thus corresponds to a physical volume of about $(2.74(4)\mathrm{fm})^3$. The residual quark mass that parameterizes the mixing of the two domain walls across the $L_s = 16$ fifth dimension is estimated to be about 0.0031. The physical strange mass is estimated as about 0.035(1) plus the 0.0031 residual mass from the squared mass ratio of kaon and Ω^-.

For the nucleon matrix element calculation reported here, 106, 98, 356 and 178 configurations are used respectively for light quark mass values of 0.03, 0.02, 0.01 and 0.005. We see a reasonable

behavior in both pion and nucleon mass in their approach to the chiral limit, as shown in Figure 1. We obtained pion masses of m_π = 0.67, 0.56, 0.42 and 0.33 GeV, and nucleon m_N = 1.56, 1.39, 1.25 and 1.15 GeV, respectively from the ensembles with the quoted light quark mass values.

Four measurements are carried out for each configuration to improve statistics, with the source set at time slices $t_0 = 0, 16, 32, 48$ or $t_0 = 8, 19, 40, 51$ except at $m_f = 0.005$. In order to reduce computational cost at $m_f = 0.005$, we employ non-relativistic quark field and a double source method where the two sources, either at $(0, 32)$ or $(16, 48)$, are set for one quark propagator. In the three-point function the source and sink operators are separated by 12 time slices to reduce excited-state contamination as much as possible.

4. Form factor results

4.1 Axial charge

Figure 2 shows our result of the axial charge normalized by Z_V. The (2.7 fm)^3 volume data are well determined and the statistical uncertainties are less than 8%. The data are almost independent of the pion mass squared except the lightest point. The lightest pion mass data is about 15% smaller than the other pion mass data. An earlier 2-flavor calculation by the RBC Collaboration [16] with the spatial volume (1.9 fm)^3 and $1/a = 1.7$ GeV showed a similar trend, but with the downward behavior setting in at a heavier pion mass than the current 2+1 flavor case.

We suspect that this pion mass dependence driving the axial charge away from the experiment at light quark mass values is caused by the finite lattice volume: In general such finite volume effect is expected to grow as we set the quark mass lighter as such lighter quarks fluctuate more. This interpretation is not inconsistent with the observed behavior of the (2+1)- (present) and 2-flavor ([16]) DWF results. Furthermore the finite volume effect is larger on smaller spatial volume when the quark mass is same. More quantitatively, we observe in the figure that the 2-flavor result from the (1.9 fm)^3 volume significantly decreases at $m_\pi = 0.24$ GeV^2, while the (2+1)-flavor results from the (2.7 fm)^3 volume does not even at $m_\pi^2 = 0.17$ GeV^2. The similar behavior was also observed in an earlier small-volume, quenched study [8].

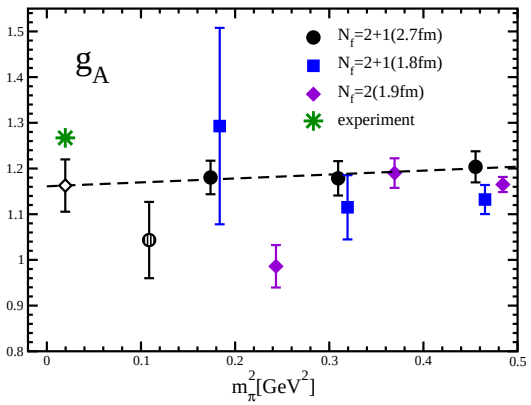

Figure 2: Axial charges with 2+1 flavor and 2 flavor. Dashed line represents linear chiral extrapolation of larger volume, 2+1 flavor data without lightest point.

Also shown in the figure is a set of (2+1)-flavor results from a smaller volume [17], $(1.8\ \mathrm{fm})^3$, with the pion mass, spatial volume and lattice spacing comparable to the 2-flavor calculations. However, the result at the lightest pion mass suffers from a large statistical fluctuation and prevents us from deciding whether there is a similar finite-size effect here.

In order to compare the results from the (2+1)- and 2-flavor calculations, we plot the axial charge against a dimensionless quantity, $m_\pi L$, as presented in the left panel of Figure 3. The (2+1)-flavor, larger volume results and the 2-flavor ones align well with each other, and suggest a monotonic dependence on $m_\pi L$: in other words, an $m_\pi L$ scaling. The (2+1)-flavor results from the smaller volume are also consistent with this $m_\pi L$ scaling except for the lightest point that suffers from large statistical fluctuation. This large statistical fluctuation itself can be another manifestation of a large finite-size effect. Nevertheless we plan to improve the statistics of this lightest point so as to test the reliability of this $m_\pi L$-scaling interpretation.

We also plot the axial charge calculated with 2 flavors of dynamical Wilson and improved Wilson quarks respectively by LHPC/SESAM [18] and QCDSF [19] collaborations against $m_\pi L$ (see the right panel in Figure 3.) These calculations were performed at various different spatial volumes, pion masses, and the gauge couplings. Like our (2+1)- and 2-flavor DWF results in the above, all of these were calculated at unitary points where the sea and valence quark masses are equal, $\kappa_{sea} = \kappa_{val}$. These Wilson quark results also seem to suggest a similar scaling in $m_\pi L$, with a downward behavior setting in at $m_\pi L$ around and below 6.

In the above we discussed that the downward shift away from the experiment of the axial charge at lighter quark mass values may well be caused by finite lattice volumes. We found the axial charge is well described by a monotonic scaling in the dimensionless parameter, $m_\pi L$. This $m_\pi L$ scaling seems common among both DWF and Wilson dynamical quark calculations performed at unitary points. Therefore, we seem to have a strong case to suspect a large finite-size effect in nucleon electroweak matrix elements in the quark mass range relevant for extrapolating to the physical or chiral point.

Thus we carry out chiral extrapolation of the axial charge using only the larger volume results and without the lightest pion mass point. We simply use a linear function of the pion mass squared, because there now are only three available data points which do not suggest any non-linear behavior

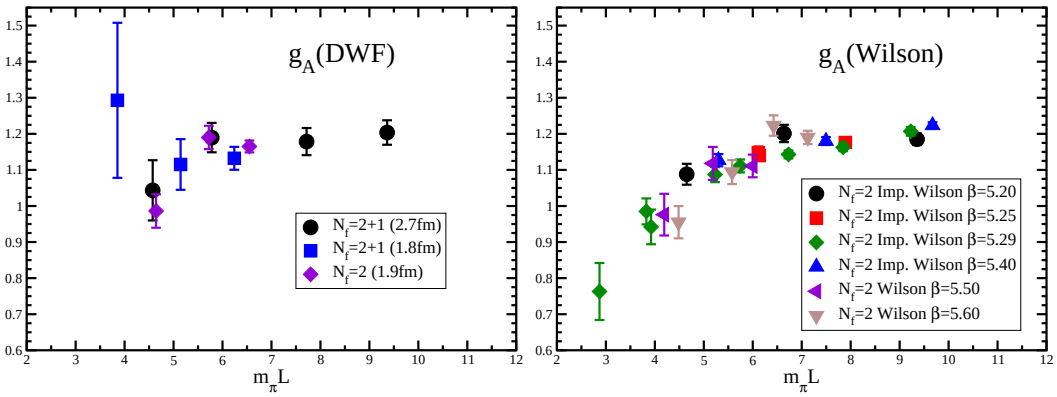

Figure 3: Axial charges with our dynamical domain wall(left panel) and dynamical Wilson fermions(right panel) obtained by LHPC/SESAM [18] and QCDSF [19] collaborations as a function of $m_\pi L$.

in the pion mass squared. The extrapolation is presented also in Figure 2: we obtain $g_A = 1.16(6)$ at the physical pion mass $m_\pi = 0.14$ GeV. This extrapolated value is 8.3% smaller than the experiment. Note this deviation may also be caused by a finite volume effect which may be present even at the heavier quark mass values used in the estimation.

We need more detailed study to clarify this possibly large finite volume effect, not only in the axial charge but also in other form factors and structure functions. We plan a larger volume calculation at the same cut off in the near future.

4.2 Isovector Dirac form factor

The left panel of Figure 4 shows our result of the isovector Dirac form factor at the four quark mass values plotted against the momentum transfer squared, q^2. The form factor is renormalized by Z_V, in other words, normalized by $1/F_1(0)$. Traditionally the experimental Dirac form factor is considered to be approximated well by a dipole form,

$$F_1(q^2) = 1/(1+q^2/M_1^2)^2, \tag{4.1}$$

where M_1 denotes the dipole mass. This traditional experimental dipole fit is shown in the figure also, represented by the dashed line with $M_1 = 0.857(8)$ GeV [7]. Thus it is convenient to fit the present, lattice-calculated Dirac form factor by the dipole form as well. The fit results are presented in the figure as solid lines for each quark mass value. With a mild dependence on the quark mass, there is tendency for the calculated results to approach the experimental line as the quark mass is decreased.

The Dirac root mean square (rms) radius is determined by the dipole mass by a relation: $\sqrt{\langle r_1^2 \rangle} = \sqrt{12}/M_1$. Thus the experimental value is 0.794(4) fm. The right panel of Figure 4 shows our results for the Dirac rms radius obtained by the dipole fit. The pion mass dependence is again mild as it was in the dipole fit discussed in the above. While the result at the lightest pion mass is trending toward the experiment with a large statistical error, we cannot exclude that large finite-size effect as discussed in the above subsection 4.1 does not affect the data. We nevertheless decided to exclude this point from our chiral extrapolation which is represented by the dashed line in the figure: we employ a linear chiral extrapolation due to the mild m_π^2 dependence of the heavier data,

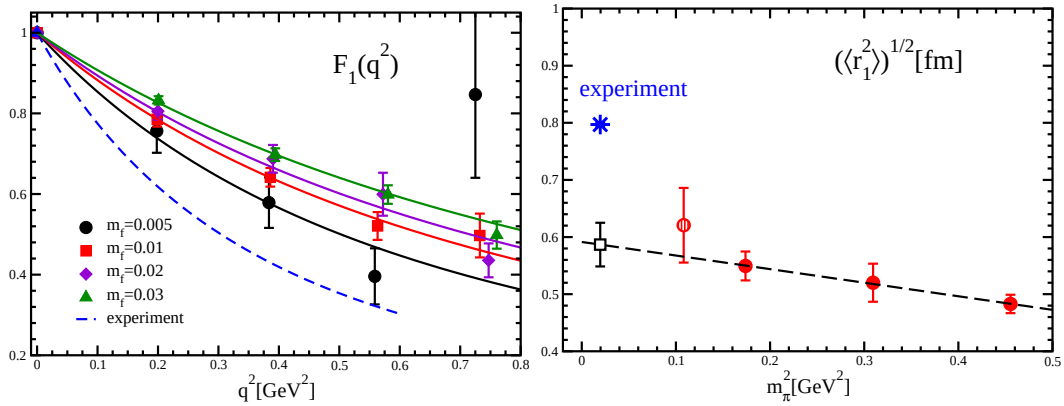

Figure 4: Isovector Dirac form factor and Dirac rms radius are presented in left and right panels, respectively. Dashed line in right panel is chiral extrapolation without lightest pion mass data.

and obtain $\sqrt{\langle r_1^2 \rangle} = 0.59(4)$ fm. The result reproduces about 74% of the experimental value at the physical pion mass. As can be seen from the figure, the lightest point is consistent with this fit with its large statistical fluctuation.

4.3 Isovector Pauli form factor

The isovector Pauli form factor is the induced tensor part of the vector current matrix element. We can calculate it at the same time with the Dirac form factor except at zero momentum transfer where the kinematics prevent us. Figure 5 presents the results of our calculation of this form factor at each quark mass plotted against the four momentum transfer squared. The form factor is renormalized by Z_V again.

The results, unlike the Dirac form factor, suffer from statistical fluctuation. Yet they can be fitted by the dipole form,

$$F_2(q^2) = F_2(0)/(1+q^2/M_2^2)^2. \tag{4.2}$$

The fit results are shown in the figure. There is a large quark mass dependence: the form factor decreases as the quark mass is decreased. The three heavier quark mass results seem to approach the experiment, shown as the dashed line with the dipole mass $M_2 = 0.78(2)$ GeV [7]. The lightest quark mass result is an exception, however. Note it suffers large fluctuation.

We determine the anomalous magnetic moment $F_2(0)$ and the Pauli rms radius $\sqrt{\langle r_2^2 \rangle} = \sqrt{12}/M_2$ from the dipole fit. Figure 6 shows the former in the left and the latter in the right panel as functions of the pion mass squared.

The anomalous magnetic moment shows only a mild mass dependence, and is almost consistent with the experiment, $F_2(0) = \mu_p - \mu_n - 1 = 3.70589$ even at the heaviest point (μ_p and μ_n are the magnetic moments of proton and neutron respectively.) Though we again cannot exclude the possibility of large finite-size effect at the lightest point, the result there is almost consistent with the linear fit to the rest which gives an extrapolation to the physical point, $F_2(0) = 3.0(5)$.

In contrast, the rms radius shows a strong mass dependence approaching the experiment as the pion mass decreases. Again we cannot exclude the possibility of large finite-size effect at the lightest point. Omitting the lightest point the linear fit gives an extrapolated rms radius of $\sqrt{\langle r_2^2 \rangle} = 0.69(9)$ fm at the physical point.

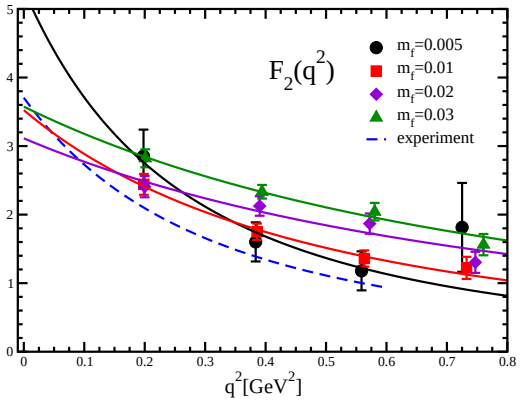

Figure 5: Isovector Pauli form factor as a function of momentum transfer squared.

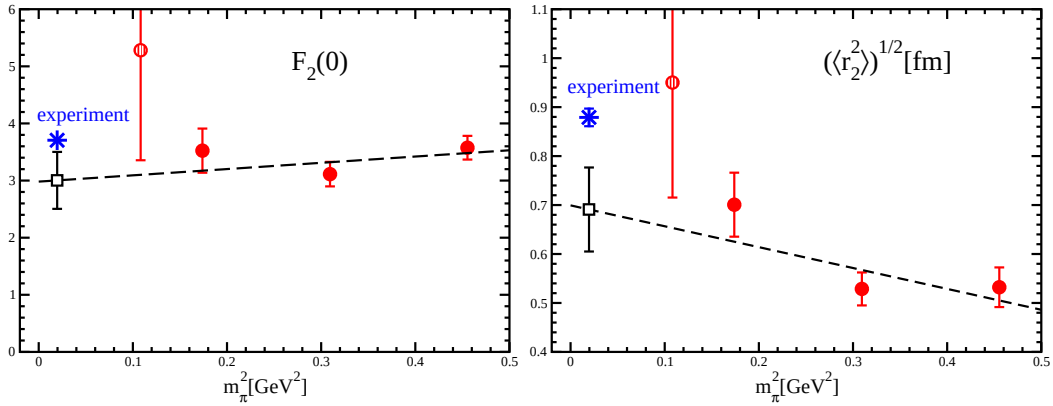

Figure 6: Pauli form factor at zero momentum transfer and Pauli rms radius are presented in left and right panels, respectively. Dashed lines are chiral extrapolations without lightest pion mass data.

These extrapolated values of anomalous magnetic moment and Pauli rms radius are about 20 % lower than the corresponding experiments. While the former almost catches the experiment within one standard deviation, the latter is about two standard deviations away.

4.4 Isovector axial vector form factor

In this section we focus only on the momentum transfer dependence of the axial vector form factor: We normalize the form factor by its value at zero momentum transfer respectively for each quark mass. The left panel of Figure 7 shows the results after these normalizations, $G_A(q^2)/G_A(0)$. The experimental form factor is again traditionally considered to be fitted well by the dipole form,

$$G_A(q^2)/G_A(0) = 1/(1+q^2/M_A^2)^2, \tag{4.3}$$

with the experiments giving $M_A = 1.03(2)$ GeV [20] for the axial vector dipole mass. The experimental fit is shown by the dashed line in the figure.

Fits to the calculations with the dipole form are represented by the solid lines and well describe the calculations for the heavier three quark mass values. The lightest quark mass results suffer large statistical errors and fluctuations. This is because the presented values are normalized by $G_A(0)$,

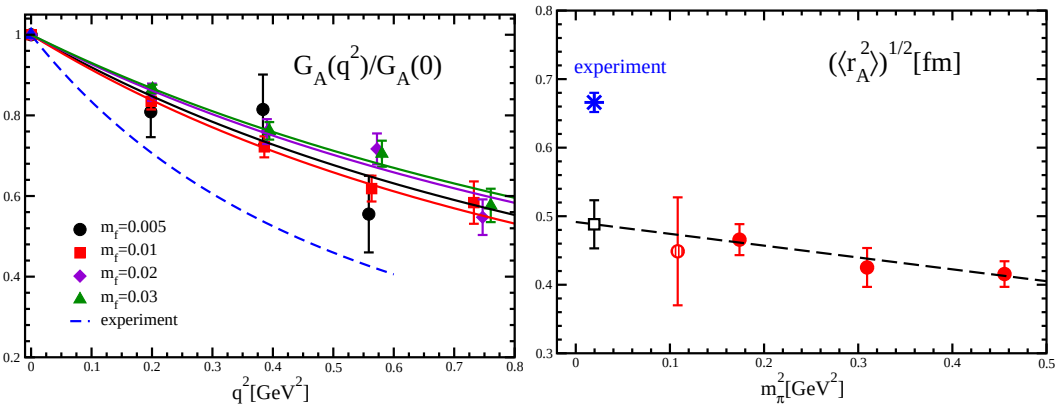

Figure 7: Isovector axial vector form factor and axial vector rms radius are presented in left and right panels, respectively. Dashed line in right panel is chiral extrapolation without lightest pion mass data.

a quantity directly proportional to the axial charge which itself suffers large statistical errors and fluctuations as discussed in the subsection 4.1. The mass dependence here is even milder than in the case of the vector current Dirac form factor.

The axial charge rms radius is determined from the dipole mass, $\sqrt{\langle r_A^2 \rangle} = \sqrt{12}/M_A$, and is 0.666(14) fm in the experiment. The calculated axial charge rms radii from the fits are shown in the right panel of Figure 7 plotted against the pion mass squared. While the result increases as the pion mass decreases, it is about 30% smaller than the experiment. The lightest pion mass data is omitted in the following chiral extrapolation, because we cannot rule out a large systematic error stemming from the suspected large finite-size effect. However the result would not change, as can be seen from the figure, if we included the point. We carry out a linear fit and extrapolation with the heavier three mass values and obtain 0.49(4) fm at the physical pion mass. The result reproduces 73% of the experiment.

4.5 Isovector induced pseudoscalar form factor

The induced pseudoscalar form factor, $G_P(q^2)$, is obtained as a part of the matrix element of the axial vector current. This form factor is expected to have a pion pole, so its momentum-transfer dependence should be different from the other form factors.

The left panel of Figure 8 shows the calculated $G_P(q^2)$ renormalized with Z_V as plotted against the momentum transfer squared at each quark mass. Note that the values at the smallest q^2 are almost 8 and much larger than other form factors. In addition, while it may be hard to observe due to large errors, the values at the smallest q^2 increase as the quark mass is decreased except at the lightest quark mass. This behavior is consistent with pion pole dominance.

The induced pseudoscalar form factor is related to the axial vector form factor through the so-called partially conserved axial vector current (PCAC) relation which is a manifestation of spontaneously broken chiral symmetry. In the traditional PCAC current algebra, the celebrated generalized Goldberger-Treiman relation,

$$G_P(q^2) = 2m_N G_A(q^2)/(q^2 + m_\pi^2), \tag{4.4}$$

is obtained at low q^2. The denominator on the right-hand side of this relation corresponds to the pion pole. We investigate the relation in our results through a quantity, $(q^2+m_\pi^2)G_P(q^2)/(2M_N G_A(q^2))$.

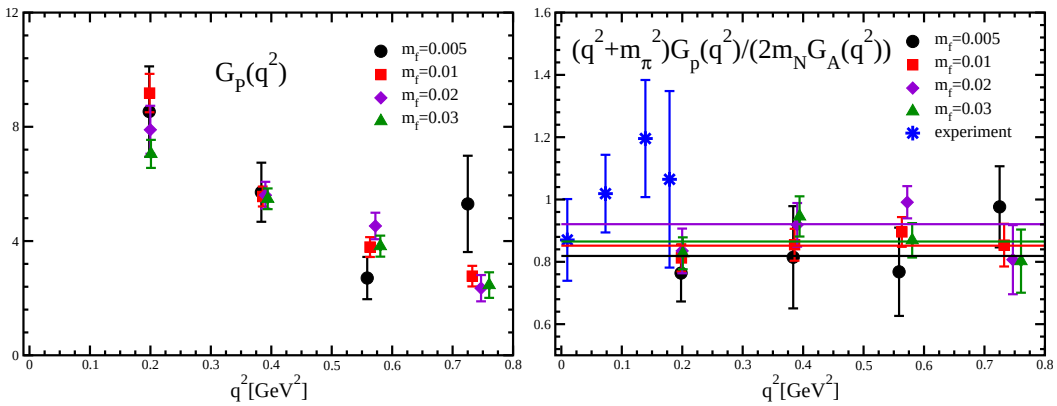

Figure 8: Isovector induced pseudoscalar form factor and ratio of pseudoscalar form factor to axial vector form factor are presented in left and right panels, respectively.

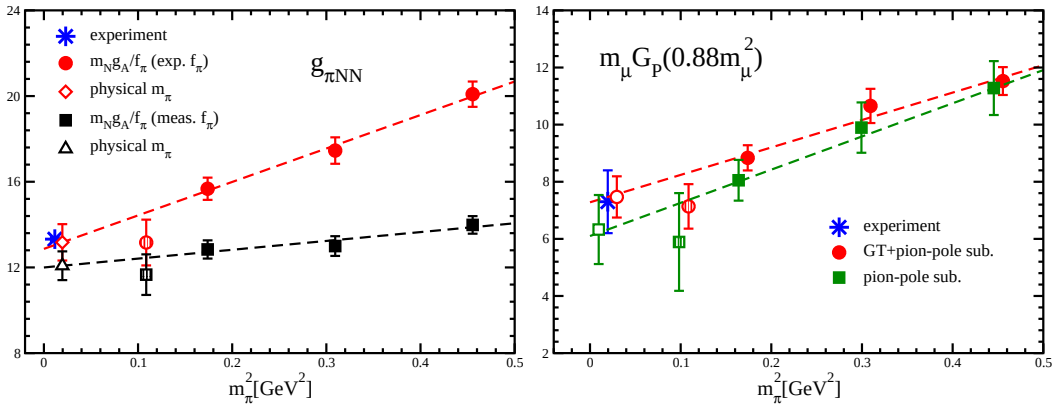

Figure 9: Left panel is the πNN coupling evaluated by GT relation with experimental and measured f_π. Right panel is induced pseudoscalar coupling for muon capture determined with generalized GT relation and induced pseudoscalar form factor. Dashed lines are chiral extrapolations without lightest pion mass data.

If the relation holds we obtain unity for this quantity. The right panel of Figure 8 shows the quantity in our calculation stays close to unity, and has no significant q^2 dependence. We can simply fit these results by a constant for each quark mass respectively, whose results are presented in the figure as well. All the fit results are consistent with the experiments [21 – 23] within the larger error of the experiments.

4.6 πNN coupling

The original Goldberger-Treiman (GT) relation [24],

$$g_{\pi NN} f_\pi = 2 m_N g_A, \tag{4.5}$$

equates a combination of quantities at the pion pole, the πNN coupling, $g_{\pi NN}$, and the pion decay constant, f_π, on the left with another combination of quantities at almost zero momentum transfer, the nucleon mass and axial charge. As such it suffers from the mismatch in momentum transfer if we substitute the experimental values for the quantities, such as $f_\pi = 93$ MeV, $m_N = 940$ MeV and $g_A = 1.269$, to obtain a value for the πNN coupling, $g_{\pi NN}$. Thus it becomes interesting how much better or worse our lattice calculation does in this regard.

In the left panel of Figure 9 we show two such calculations each for the πNN coupling, $g_{\pi NN}$: one uses the experimental value of f_π and another the lattice-calculated values at each quark mass, plotted against the pion mass squared. The results with the experimental f_π exhibit a significant slope in terms of m_π^2, while that with the calculated f_π is almost flat. In both methods the results at the lightest mass show significant downward shift away from the trend set by the three heavier mass values. This of course is another manifestation of the large deviation observed in the axial charge which was discussed in detail in subsection 4.1. For the chiral extrapolation we simply employ a linear fit form and exclude the lightest mass point. We obtain the results at the physical pion mass, $g_{\pi NN} = 13.2(9)$ with the experimental f_π and $g_{\pi NN} = 12.1(7)$ with the calculated f_π. The extrapolated results at the physical pion mass are consistent with the experiment obtained from forward π-N scattering data [25].

4.7 Muon capture

The induced pseudoscalar coupling, $g_P = m_\mu G_P(q_c^2)$, is defined with the muon mass m_μ and the induced pseudoscalar form factor G_p at the momentum transfer squared, $q_c^2 = 0.88 m_\mu^2$ GeV^2. This is for convenience in application for muon capture, $p + \mu^- \to n + \nu_\mu$, where the two-body nature of the process defines the momentum transfer, q_c.

$G_P(q^2)$ can be described by the pion pole dominance form through the generalized Goldberger-Treiman relation (4.4), and a constant α which corresponds to the difference from unity of the quantity, $(q^2+m_\pi^2)G_P(q^2)/(2M_N G_A(q^2))$, at each quark mass. These were summarized in Figure 8. Thus, g_P is determined by

$$g_P = \alpha m_\mu \frac{2m_N G_A(q_c^2)}{q_c^2+m_\pi^2} = \alpha m_\mu \frac{2m_N}{q_c^2+m_\pi^2}\frac{g_A}{(1+q_c^2/M_A^2)^2}, \tag{4.6}$$

where we use the dipole form of the axial vector form factor (4.3). In order to subtract the strong pion mass dependence stemming from the pion pole, we use the physical pion mass in the pion pole. On the other hand we use the calculated values for m_N, g_A, M_A and α. The right panel of Figure 9 shows that the result denoted by circle is almost linear as a function of the pion mass squared and decreases toward the experiment for the three heavier mass values. Again the lightest mass result is an exception: We suspect the significant drop here at the lightest point is caused by the finite volume effect in g_A as discussed in Sec. 4.1.

We also determine g_P from $G_P(q^2)$ directly with the subtraction of the pion pole. At each quark mass the quantity $G_P(q^2)(q^2+m_\pi^2)$ is fitted by the dipole form, and then extrapolated to q_c^2. In the figure the extrapolated result to q_c^2 normalized by the pion pole with the physical pion mass is presented by square symbol. The result from $G_P(q^2)$ has larger error, whilst the two results agree within the statistical errors at each pion mass. We carry out chiral extrapolations with a simple linear function of the pion mass squared without the lightest mass. The results at the physical pion mass are consistent with each other, and also with the recent experiment [21] and analysis[22].

5. Low moments of the structure functions

5.1 Quark momentum and helicity fractions

Let us first discuss the naturally renormalized ratio of the isovector quark momentum fraction $\langle x\rangle_{u-d}$ to helicity fraction $\langle x\rangle_{\Delta u-\Delta d}$. Since the two fractions are related with each other by a chiral rotation, they share a common renormalization. And because the DWF quarks preserve the chiral symmetry very well, as parameterized by our small residual mass of 0.0031, the ratio is naturally renormalized on the lattice. Our results are summarized in Figure 10. The ratio does not show any appreciable dependence on the quark mass, albeit with large statistical errors, and is in agreement with the experimental value. The constant fit result with all four pion mass data, $\langle x\rangle_{u-d}/\langle x\rangle_{\Delta u-\Delta d} = 0.81(2)$, is also consistent with the experiment.

Each of the fractions itself, unlike the ratio, is yet to be renormalized, but suggests interesting behavior as shown in Figure 11. They both trend down toward the experimental value at the lightest quark mass, after staying almost constant for the three heavier mass values. This may well be related to the finite-size effect we suspect for the form factor values, but not necessarily so as the

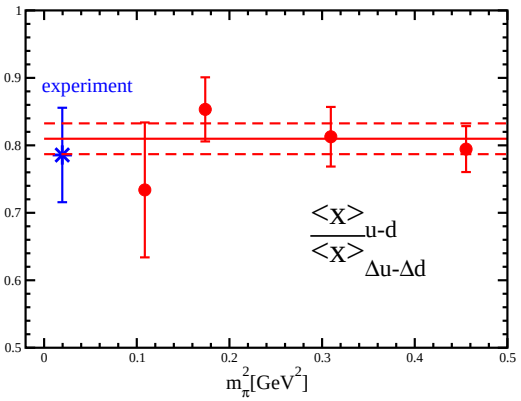

Figure 10: The naturally renormalized ratio of the isovector quark momentum fraction $\langle x \rangle_{u-d}$ to helicity fraction $\langle x \rangle_{\Delta u - \Delta d}$.

structure functions probe different, deep inelastic, physics from the elastic form factors. We will be better able to discuss these quantities after finishing the lattice non-perturbative renormalizations for them in the near future.

5.2 Transversity

The transversity, $\langle 1 \rangle_{\delta u - \delta d}$, can be measured by the RHIC Spin experiment in the near future. In the present calculation it shows a similar behavior with the quark momentum and helicity fractions: it stays almost constant for the three heavier quark mass values and then trends down at the lightest mass (see the left panel of Figure 12.) This quantity is also yet to be renormalized, but will soon be, and then will provide a prediction for the experiments planned in the near future [26].

5.3 Twist-3 d_1 moment

The d_1 moment of the twist-3 part of the polarized structure function, according to Wandzura and Wilczek [27], is small when it is calculated perturbatively. It need not be small under a non-perturbative, confining environment within the nucleon. Our calculation for this d_1 moment is summarized in the right panel of Figure 12. The result suggests, though again not renormalized

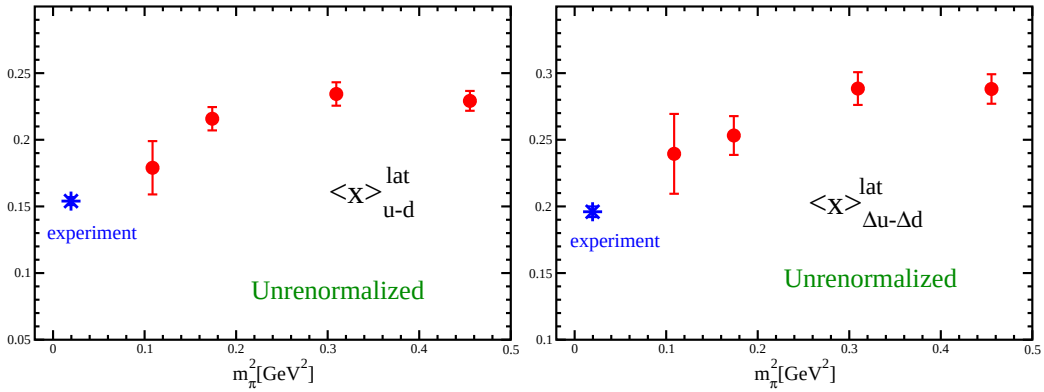

Figure 11: The isovector quark momentum fraction $\langle x \rangle_{u-d}$ (left) and helicity fraction $\langle x \rangle_{\Delta u - \Delta d}$ (right), both yet to be renormalized.

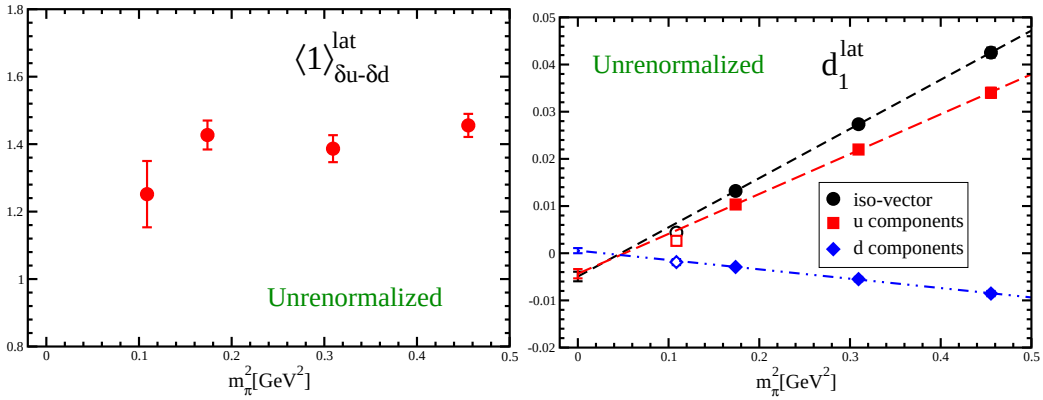

Figure 12: Transversity, $\langle 1 \rangle_{\delta u-\delta d}$, (left) and twist-3, d_1, (right) moments, unrenromalized.

yet, that it is small, consistent with Wandzura and Wilczek. We note also that the results at the lightest quark mass show some deviation from the linear extrapolations from the three heavier mass values.

6. Conclusions

We calculated the isovector form factors and low moments of structure functions of the nucleon with $N_f = 2+1$ dynamical domain wall fermions at 1.7 GeV cutoff on a $(2.7\ \mathrm{fm})^3$ spatial volume. The axial charge at the lightest quark mass is about 15% smaller than the other mass data, and it seems affected by a finite volume effect. It scales with a single parameter, $m_\pi L$, the product of pion mass and the linear spatial lattice size. We confirmed similar scaling in earlier $N_f = 2$ dynamical DWF and Wilson fermion calculations. Without the lightest point the axial charge is estimated as 1.16(6) by a linear extrapolation to the physical point. The root mean square radii for the form factors except the induced pseudoscalar are determined and at the physical pion mass are 20–30% smaller than experiments. The πNN coupling and induced pseudoscalar coupling are found to be consistent with experiments.

We found the renormalized ratio of the isovector quark momentum fraction $\langle x \rangle_{u-d}$ to helicity fraction $\langle x \rangle_{\Delta u-\Delta d}$ is in agreement with experiment. Their individual values, though yet to be renormalized, show an encouraging trend toward the experimental values at the lightest quark mass. Their non-perturbative renormalization will be completed soon. We calculated the bare transversity which will provide a prediction when its non-perturbative renormalization is completed in the near future. We found the twist-3 d_1 moment is small, consistent with the Wandzura-Wilczek relation.

Acknowledgments

We thank the members of the RBC and UKQCD collaborations, present and past, especially T. Blum, H. W. Lin, S. Sasaki and J. Zanotti. We also thank RIKEN, Brookhaven National Laboratory, University of Edinburgh, UK PPARC and the U.S. DOE for providing the facilities essential for conducting this research. T.Y. is supported by US DOE grant DE-FG02-92ER40716 and the University of Connecticut.

References

[1] D. J. Antonio *et al.* [RBC and UKQCD Collaborations], Phys. Rev. **D75** (2007) 114501 [arXiv:hep-lat/0612005].

[2] C. Allton *et al.* [RBC and UKQCD Collaborations], Phys. Rev. **D76** (2007) 014504 [arXiv:hep-lat/0701013].

[3] D. J. Antonio *et al.* [RBC and UKQCD Collaborations], arXiv:0705.2340 [hep-lat].

[4] D. B. Kaplan, Phys. Lett. **B288** (1992) 342.

[5] Y. Shamir, Nucl. Phys. **B406** (1993) 90.

[6] V. Furman, and Y. Shamir, Nucl. Phys. **B439** (1995) 54.

[7] W.-M. Yao *et al.*, J. Phys. **G33** (2006) 1.

[8] S. Sasaki *et al.*, Phys. Rev. **D68** (2003) 054509 [arXiv:hep-lat/0306007].

[9] S. Sasaki and T. Yamazaki, arXiv:0709.3150 [hep-lat].

[10] K. Orginos *et al.*, Phys. Rev. **D73** (2006) 094503 [arXiv:hep-lat/0505024].

[11] P. Hägler *et al.* [LHPC Collaboration], Phys. Rev. **D68** (2003) 034505 [arXiv:hep-lat/0304018].

[12] T. Blum *et al.*, Phys. Rev. **D66** (2002) 014504 [arXiv:hep-lat/0102005].

[13] P. A. Boyle *et al.*, IBM J. of Res. and Dev. **49** (2005) 351.

[14] Y. Iwasaki, UTHEP-118, unpublished.

[15] M. F. Lin and E. E. Scholz [RBC and UKQCD Collaborations], PoS(LAT2007) (2007) 120.

[16] H. W. Lin *et al.* [RBC Collaboration], in preparation.

[17] [RBC and UKQCD Collaborations], in preparation.

[18] D. Dolgov *et al.* [LHPC Collaboration], Phys. Rev. **D66** (2002) 034506 [arXiv:hep-lat/0201021].

[19] A. Ali. Khan *et al.*, Phys. Rev. **D74** (2006) 094508 [arXiv:hep-lat/0603028].

[20] V. Bernard *et al.*, J. Phys. **G28** (2002) R1 [arXiv:hep-ph/0107088].

[21] V. A. Andreev *et al.* [MuCap Collaboration], Phys. Rev. Lett. **99** (2007) 032002 [arXiv:0704.2072 [nucl-ex]].

[22] A. Czarnecki *et al.*, Phys. Rev. Lett. **99** (2007) 032003 [arXiv:0704.3968 [hep-ph]].

[23] S. Choi *et al.*, Phys. Rev. Lett. **71** (1993) 3927.

[24] M. L. Goldberger and S. B. Treiman, Phys. Rev. **110** (1958) 1178.

[25] T. E. O. Ericson *et al.*, Phys. Rev. **C66** (2002) 014005 [arXiv:hep-ph/0009312].

[26] M. Grosse Perdekamp, private communication.

[27] S. Wandzura and F. Wilczek, Phys. Lett. **B72** (1977) 195.